Vorticity Based Flow Analysis and Visualization for Pelton Turbine Design Optimization

Filip Sadlo[1]   Ronald Peikert[1]   Etienne Parkinson[2]

[1]ETH Zürich   [2]VA Tech Hydro

ABSTRACT

Vorticity is the quantity used to describe the creation, transformation and extinction of vortices. It is present not only in vortices but also in shear flow. Especially in ducted flows, most of the overall vorticity is usually contained in the boundary layer. When a vortex develops from the boundary layer, this can be described by transport of vorticity. For a better understanding of a flow it is therefore of interest to examine vorticity in all of its different roles. The goal of this application study was not primarily the visualization of vortices but of vorticity distribution and its role in vortex phenomena.

The underlying industrial case is a design optimization for a Pelton turbine. An important industrial objective is to improve the quality of the water jets driving the runner. Jet quality is affected mostly by vortices originating in the distributor ring. For a better understanding of this interrelation, it is crucial to not only visualize these vortices but also to analyze the mechanisms of their creation.

We used various techniques for the visualization of vorticity, including field lines and modified isosurfaces. For field line based visualization, we extended the image-guided streamline placement algorithm of Turk and Banks to data-guided field line placement on three-dimensional unstructured grids.

CR Categories: I.3.8 [Computer Graphics]: Applications; I.4.7 [Image Processing and Computer Vision]: Feature Measurement - Feature Representation; J.2 [Applications]: Physical Sciences and Engineering - Engineering.

Keywords: flow visualization, feature extraction, line placement.

1 INTRODUCTION

A Pelton turbine is a hydraulic turbine where the runner is rotating from the impulse of water jets on its buckets. The water exits the manifold via its injectors (see Fig. 1 and Fig. 2).

As known from experience [23], the characteristics of the water jets have a direct impact on the efficiency of the hydraulic turbine. Indeed, the jet does not necessarily follow the injector's geometrical axis, can show a non-cylindrical shape and has a dispersed mixed air / water zone on its boundary.

These hydrodynamic patterns are mostly consequences of the flow characteristics in the injector, which itself results from the main pipe flow after the bifurcation where the flow is deviated towards the injector. This flow deviation, together with the bend in the main pipe, induces complex vortex structures in the injectors.

The characteristics of these vortices in size, intensity and spatial distribution appear to be key control parameters of the jet "quality". Consequently, a strong interest lies in the identification and detection of these vortices. Their energetic intensity classification is also an important factor as it helps in identifying the "key" vortices with respect to the jet quality, and thus the related design optimization that could be investigated to minimize / eliminate their negative effects.
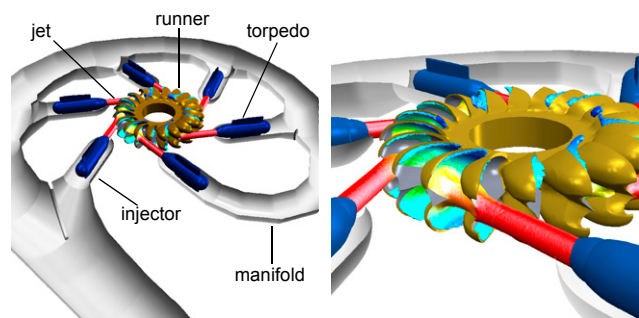

Figure 1: Pelton turbine: Manifold, injectors, torpedoes, jets and runner.

Figure 2: Detail of jet hitting buckets, colored by kinetic energy.

The extraction of vortices from steady flow data has been investigated by many researchers. In most of recent literature, vortices are approached via the shape of a streamline bundle. The vortex shape has been described in topological [12] or geometrical terms [18,29] or by templates [8]. The shape of a streamline pattern is not Galilean invariant, but depends on the frame of reference. Shape-based methods have been used successfully for various types of, mostly longitudinal, vortices. The methods fail however on vortices which need to be observed in a moving frame of reference. A classical example are the hairpin vortices occurring in boundary and mixing layers. Methods for their detection must be formulated independent of the reference frame, i.e. they must not include the constant term of the velocity. Reportedly ([7]), the method giving the sharpest extraction results for this type of vortices is the λ_2 method [15].

There exist several vortex criteria which are Galilean invariant. A necessary criterion is the presence of complex eigenvalues of the velocity gradient tensor ∇u [4,11]. In practice, this is usually not sufficient for the isolation of single vortices. Other proposed criteria are high vorticity [28], low pressure [22] the combination of low pressure and high vorticity [1], and low pressure and positive second invariant Q of ∇u [14].

Even more challenging than moving vortices are quickly deforming vortices. While by Helmholtz' vortex theorems (see e.g. [2]) vorticity is conserved for inviscid flow (and approximately for flows under investigation), vorticity distribution may change

rapidly, in particular, vortex sheets can separate from the boundary and roll up.

In Section 2, we give some background on the physics involved in the presence of vortices and vorticity. Then, in Section 3, we propose some novel tools for interactive exploration of a flow aimed not only at the shape of flow features but at their physical understanding. We give an evaluation of the tools in Section 4, in the context of the Pelton turbine optimization study currently being done by VA Tech Hydro.

2 BACKGROUND ON VORTICES AND VORTICITY

A well known difficulty in the discussion of vortices is the lack of a formal definition. Robinson extended Lugt's working definition of a region of closed or spiralling streamlines by the requirement that the observer must move with the average velocity measured at the vortex core [19,25]. By its implicit nature, this definition is difficult to apply, and its room for interpretation led to a variety of vortex criteria, even if the scope is narrowed to strictly physical criteria. We give an overview in this section, and we discuss direct visualization of the vorticity field.

2.1 Physically Based Vortex Indicators

A number of well known criteria for the presence of a vortex or, more generally, a swirling flow are derived immediately from the Navier-Stokes equation. For incompressible flow, the Navier-Stokes equation is

$$\frac{D\boldsymbol{u}}{Dt} = -\frac{1}{\rho}\nabla p + \nu\nabla^2\boldsymbol{u} \tag{1}$$

where the left hand side is the material derivative of the velocity, i.e. the acceleration, ρ is the constant density, p is pressure and ν is the constant kinematic viscosity.

It is worth noticing that the divergence, curl and gradient operators, when applied to Eq. 1, all yield equations which are relevant for visualization.

• The *divergence* of Eq. 1 is the scalar equation

$$\nabla\bullet\left(\frac{D\boldsymbol{u}}{Dt}\right) = -\frac{1}{\rho}\nabla^2 p \tag{2}$$

having made use of the (incompressible) continuity equation $\nabla\bullet\boldsymbol{u} = 0$. A positive Laplacian of pressure is a well-known vortex indicator [7]. The pressure Laplacian is up to a constant factor identical to the second invariant Q of the velocity gradient tensor $\nabla\boldsymbol{u}$ which is the basis of Hunt's vortex criterion. Eq. 2 gives yet another, and quite intuitive, formulation: Instead of looking for low pressure regions, we can equivalently look for regions of high convergence of the acceleration field.

• The *curl* of Eq. 1 is the well-known vorticity equation

$$\frac{D\omega}{Dt} = (\omega\bullet\nabla)\boldsymbol{u} + \nu\nabla^2\omega \tag{3}$$

where ω is the vorticity $\nabla\times\boldsymbol{u}$. It describes the rate of change of a particle's vorticity by vortex stretching and by vorticity diffusion. The fact that the pressure has disappeared makes Eq. 3 an attractive alternative to Eq. 1 for flow simulations and has led to the so-called vortex methods [5]. In visualization, this equation allows to separately visualize vortex stretching and vorticity diffusion.

• The *gradient* of Eq. 1 is the matrix equation

$$\nabla\frac{D\boldsymbol{u}}{Dt} = -\frac{1}{\rho}\nabla\nabla p + \nu\nabla\nabla^2\boldsymbol{u} \,. \tag{4}$$

It is the basis for the λ_2 vortex criterion [15], which is derived as follows. The pressure Hessian is a symmetric matrix, it therefore suffices to take the symmetric part of Eq. 4:

$$\frac{D\boldsymbol{S}}{Dt} - \nu\nabla\nabla^2\boldsymbol{S} + \boldsymbol{S}^2 + \Omega^2 = -\frac{1}{\rho}\nabla\nabla p \tag{5}$$

where S is the symmetric and Ω the antisymmetric part of the matrix $\nabla\boldsymbol{u}$. After removing terms one (unsteady irrotational straining) and two (viscous effects), the remaining part of the pressure Hessian is essentially the symmetric matrix $S^2+\Omega^2$. If its three eigenvalues are ordered as $\lambda_1 \geq \lambda_2 \geq \lambda_3$, the criterion for λ_2 is $\lambda_2 < 0$ which means that the pressure function graph has positive curvature in at least two orthogonal directions.

A few other methods are not directly linked to the Navier-Stokes equations, such as the extraction of extremum lines of (low) pressure [22] or (high) vorticity magnitude [28]. Finally, the most prominent vortex criterion which is *not* Galilean invariant is helicity, the cross product of velocity and vorticity. Normalized helicity (also called helicity density) is the often used variant obtained by first dividing the velocity and vorticity vector by their lengths.

2.2 Vorticity Field Lines

Visualization of the vorticity field appears to be a powerful approach to the visualization and understanding of vortices and their creation. Vorticity is present in any vortex and it often gives a simpler representation because of the rotational nature of vortices. Although vorticity is also present in vortex-free regions like boundary shear flow, these regions often play an important role in the creation of vortices. Therefore, the complete vorticity field is visualized. This can for example help the understanding of how boundary shear flow detaches and contributes to vortices.

Isosurfaces of vorticity magnitude are often used for the visualization of vortices [27]. However, the direction of vorticity is lost by this technique. Therefore, and because of the possible transition from shear flow to a vortex and the fact that the extent of a vortex (its hull) is not clearly defined, we propose the visualization of vorticity field lines as a complementary method.

Because of the analogy between vorticity fields and magnetic fields (field lines are closed, terminated by a boundary or of infinite length), we decided to use a corresponding visualization technique for the vorticity field. Magnetic fields are usually visualized by closed (maximal length) field lines with line density proportional to the magnitude of the field. This familiar property of magnetic fields holds for all divergence-free vector fields and thus for vorticity. The reason is that by Gauss' theorem the total flux through a closed surface is zero for a divergence-free field. Hence for a stream tube segment, the fluxes through the two cross sections are equal which implies that average magnitudes are inversely proportional to projected surface and therefore proportional to the field line density.

From an algorithmic point of view, a set of field lines with this density property can be achieved by using a modification of the streamline placement algorithm of Turk and Banks [31], as is described in Section 3.3. To support the interpretation of the flow, the vorticity field lines are colored by scalar quantities as shown in Section 4.2.

3 TOOLS FOR EXPLORATIVE VISUALIZATION

For interactive exploration of flows and their vorticity fields, we developed a set of tools which we will describe in this section. These tools are mainly designed for usage in the Cykloop virtual environment [33] installed at VA Tech Hydro's site, therefore we aimed at mostly automatic methods with little user input other than the picking of objects. The field line placement described in Section 3.3 requires a preprocessing of the dataset.

3.1 Analysis of Vortex Cores

A good first step to approach a new CFD dataset is to run a vortex core line extraction. The methods we use for core line extraction are those by Levy et al. [18] and by Sujudi and Haimes [29]. We suppress false positives and weak vortices as described in [24].

Vortex cores are inherent properties of the velocity field and do not depend on parameter choices as would be the case for isosurfaces. The strength of vortex core algorithms lies in their ability to isolate nearby vortices. Their weakness is that the obtained information is strictly local. Further steps are needed to get information such as the spatial extent of a vortex or the relative importance of nearby vortices. Importance can be defined in terms of kinetic energy, of occupied space or other criteria, depending of the application.

There exist automatic methods for reducing the number of obtained features based on clustering [6,30], or on scale-space analysis [3]. For a more thorough analysis of groups of vortex cores, we developed a simple tool which proved to be useful. The tool allows the user to pick a core line which he or she wants to analyze. A circle of seed points is then centered at the pick location such that its axis is aligned with the velocity vector. From this circle, a stream tube is generated in one or both directions by using Hultquist's algorithm [13]. The radius of the seed circle can be adjusted manually. Fig. 3 shows the streamline seeding tool being used to study the main vortex at the bifurcation to the first injector.

This semi-automatic analysis step resembles the verification techniques in [16] and [10]. It is important to note that any such verification technique is subject to interpretation. The reason is: It cannot be expected that a stream tube follows the vortex core line over an extended time. Even if a stream line coincides with the core line for a while, it may later start to wind around it, and a different streamline takes over the role of best matching the core line. This situation, sketched in Fig. 4, was met in practice (Fig. 9).
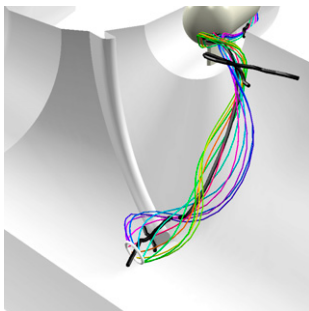

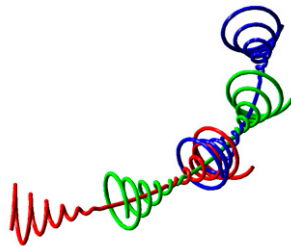Figure 3: Vortex core, seeding circle and stream tube.

Figure 4: Sketch of vortex core approximately followed by successive streamlines.

3.2 Analysis of Vorticity Magnitude

The simplest model of a laminar viscous flow through a circular pipe (of radius R and length L) is the so-called Hagen-Poiseuille flow

$$u = -\frac{p_0 - p_1}{4\nu\rho L}(R^2 - r^2) \qquad v = w = 0 \qquad (6)$$

Its vorticity field has magnitude

$$\omega = \frac{p_0 - p_1}{2\nu\rho L}r \qquad (7)$$

which is increasing linearly towards the boundary. In practical flow fields the same behavior can be observed in the boundary layer. Often the highest vorticity magnitudes can be found near solid boundaries rather than within vortices.

It is not the absolute values of the vorticity magnitude which are of interest but rather their deviation from the "expected" behavior. This explains why vorticity isosurfaces give usually poor results for ducted flow. On the other hand, isosurfacing is a convenient tool for interactive data visualization. A simple way out of this dilemma is to apply constraints to isosurfaces. Such constraints can be any inequalities for additional data channels, such as the requirement for a minimum helicity or a minimum (or maximum) distance from solid boundaries.

A seeming disadvantage of such a "conditional isosurface" is that it is no more a closed surface. This can however be fixed by taking pairs of such surfaces:

$$\{x \mid f(x) = f_0 \wedge g(x) \geq g_0\} \cup \{x \mid g(x) = g_0 \wedge f(x) \geq f_0\} \qquad (8)$$

Any combination of inequality signs is of course possible.

The "conditional isosurfaces" proved useful for isolating interesting regions of high vorticity. We observed that features obtained by specifying a minimum vorticity magnitude and a minimum wall distance are quite similar to those obtained by λ_2 (see Fig. 7 and Fig. 8). However, λ_2 tends to be too accepting, i.e. poor in separating vortices. For that reason, the level of the λ_2 isosurface is commonly set to some value well below zero. But in a strict sense, this is not allowed as zero is the only meaningful level.
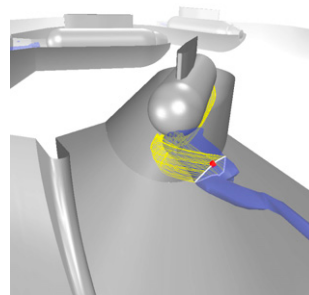

Figure 5: Isosurface of vorticity, clipped at 20 mm distance from solid boundaries. Picked point (red), planar curve (white) and streamlines.
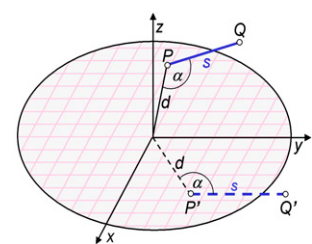
Figure 6: Filter lookup for the 3D line segment PQ by rotating the triangle 0PQ onto the xy-plane.

For the further analysis of such high vorticity regions, we adapted the streamline seeding tool of Section 3.1. From the surface point picked by the user, a planar intersection curve is computed through the isosurface. The curve is restricted to a single

component, and it is closed if the surface is closed. The normal to the intersection plane adjusts automatically to the average velocity direction. This seeding tool can be used to generate stream tubes and vorticity tubes (see Fig. 5).

3.3 Field Line Placement

For the generation of vorticity field lines with line density proportional to vorticity magnitude, we extended the iterative streamline placement algorithm of Turk and Banks [31] to three-dimensional unstructured grids and applied some additional modifications. The reason for not using single-pass methods like [9,17,21,32] is that the requirement of a prescribed non-constant line density (Section 2.2) seems easier to meet by iterative methods.

The algorithm of Turk and Banks maintains a low-pass filtered version of the streamline image for the representation of line density. Streamline placement is done by minimization of an energy function. The energy function is defined as the sum of squared error between the low-pass image and the target line density. Minimization is done by random descent using a set of operations that only take effect if energy is reduced:

• Insert: A streamline is generated and tried to be added.

• Remove: Try to remove a streamline.

• Move: Try to move a streamline.

• Lengthen, shorten, combine: Try to lengthen or shorten a streamline or to combine two streamlines to a single streamline if their ends are near enough.

The optimization process is accelerated by an oracle that tells which operation on which streamline is supposed to reduce most energy.

For the extension to three-dimensional unstructured grids, only few modifications have to be applied:

• First we have to switch from image-guided placement to data-guided placement because we want the lines to be distributed independently of the view and guided by an additional field, in our case vorticity magnitude. In the 2D algorithm of Turk and Banks, the low-pass image is generated only from the streamlines without accessing any field data, therefore the algorithm is not bound to any grid geometry or topology. We use a three-dimensional unstructured low-pass field with grid geometry identical to the vorticity field because we want to control the line density by a field derived from the vorticity field.

• We also have to adapt the low-pass filter to three dimensions. In the 2D algorithm, evaluation of the radially symmetric filter contribution is simplified by rotating the streamline segments around the filter origin to become parallel to the y-axis. Following this idea, we first rotate the 3D line segments onto the xy-plane (Fig. 6) and give that as input to the filter lookup of the 2D algorithm. This way, we effectively apply a radially symmetric 3D filter. Due to the unstructured grid geometry, we decided not to adapt the energy function as in [20] but to use this filter in physical space. As a consequence, we need an efficient point location algorithm to find the grid nodes that a line segment can contribute to, when it is low-pass filtered.

The above two modifications yield a 3D version of the streamline placement algorithm. If the interest is however to visualize divergence-free fields, the vector magnitude can be used as the target density for the placement of field lines. Possible applications include vorticity fields, velocity fields of incompressible flow, and magnetic fields. It has the advantage that field lines of maximal length can be used (Section 2.2), giving a more consistent visualization and obviating the need for lengthening, shortening and combine operations. Another advantage is the reduction of occlusion, since the user will usually scale the target density field so that there will be almost no lines in regions of low target density. For the control of line density by another field, the following modification has been chosen:

• The algorithm of Turk and Banks is mainly designed for streamline placement with constant density. It uses a target gray level, constant over the image, that has to be approximated by the low-pass image. Line density can be controlled by variation of the filter radius using an image that defines a filter radius for every point. Because we want to approximate line density given by a field, we have chosen to use a constant filter radius and to use the given field as target low-pass level instead. Overall line density can be adjusted by scaling of the density field.

In this first approach, we decided to omit the oracle for the optimization operations. We decided to do so for preventing systematic errors in the line placement. Although we implemented a (greedy) oracle for the insert operation, we switched it off to prevent placement errors and because the resulting speedup was not that significant (because extensive use of the insert operation is done only at the beginning of optimization).

4 RESULTS

The datasets in the focus of this application study are CFD simulations of the (scaled model) components of a Pelton water turbine. The simulations were computed by VA Tech Hydro using the commercial CFX-TASCflow solver. For the manifold and injectors a steady flow was computed, while for the jet and the flow in the bucket, time-dependent two-phase simulations have been done. All these simulations were performed for several different operating points. For the manifold and for the runner, symmetry planes were assumed and used as boundary conditions.

In the following, we will focus on the vortices occurring in the bifurcations of the manifold which are being studied with highest priority. It is planned as a next step to extend the analysis to the jets.

4.1 Vortex Analysis

The strongest vortices present in the distributing manifold are separation vortices at the bifurcations. Although there is one such vortex per bifurcation, they differ significantly in their shapes and especially in their interaction with other vortical structures.

At the first bifurcation, the vortex core extraction yields a set of three lines running almost parallel at some point. Possible interpretations include (a) separate vortices, (b) one main vortex and other vortices either joining or leaving it, (c) one vortex with noisy core region. Interpretation (c) is often the correct one, as can be verified by a scale-space analysis. Vorticity magnitude, when combined with minimal wall distance, is only able to indicate the interesting region, but fails to isolate vortices (Fig. 7). Isosurfaces of λ_2, giving a sharper picture, do not indicate separate vortices, regardless of the chosen level (Fig. 8). The hypothesis of separate vortices can be verified by integrating stream tubes seeded on a small circle around the core line (Fig. 9). The streamlines of each tube clearly wind around the core line. Such an analysis is however too localized and does not account for the radial extent of vortices. By backward integrating from a seed circle of an appropriate (experimentally found) radius, we got a very thin stream tube hitting the wall and spreading to a wide opening angle of streamlines running along the wall (Fig. 10). The most plausible interpretation is therefore that of two separate vortices, namely the expected strong separation vortex plus a minor vortex apparently generated by a vortex sheet rolling up.
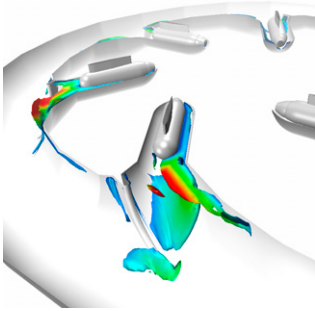
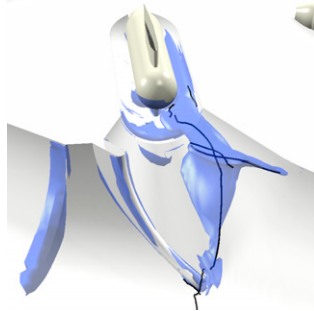Figure 7: Vorticity isosurface, wall distance d > 5 mm. (blue = 0 mm, red = 50 mm).

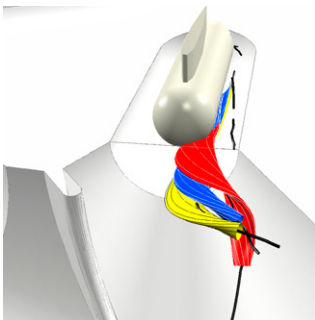Figure 8: Vortex cores near first injector, λ_2 isosurface.

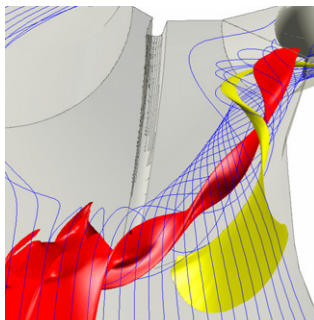Figure 9: Local "verification" of three vortex cores by stream tubes.

Figure 10: Forward and backward stream tubes reveal one separation vortex and one vortex sheet roll-up.
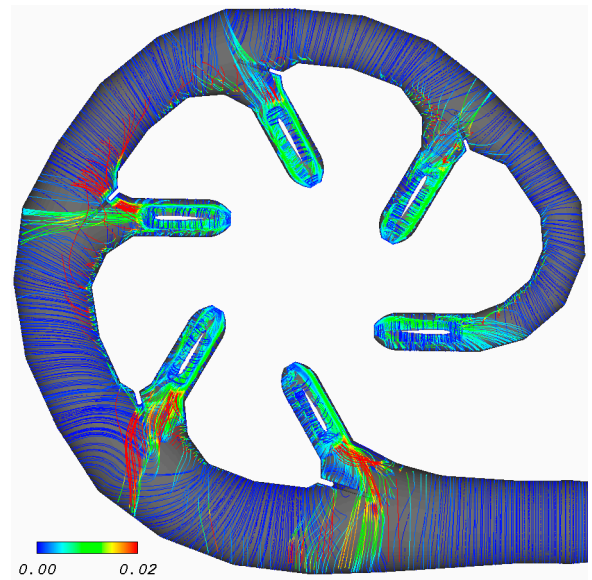

Figure 11: Top view of vorticity field lines colored with distance to boundary (in meters).
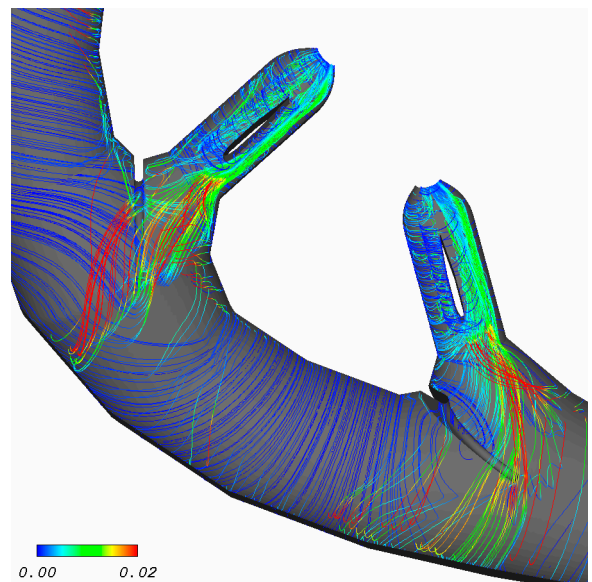
Figure 12: Closer look at the first two injectors, field lines colored with distance to boundary.

4.2 Vorticity Field Line Results

For better visualization and to support interpretation, we color the field lines with scalar quantities, for example:

- For the visualization of vortices, the field lines are colored with vortex indicators like helicity, λ_2 or pressure.
- For the discrimination between field lines of the boundary flow and field lines of the inner flow, the lines are colored with Euclidean distance to the boundary. This also shows where field lines detach from the boundary.
- For studies of the vorticity field and its role in vortex phenomena, the field lines are colored with vorticity magnitude.

All images of this section show vorticity field lines with line density proportional to vorticity magnitude. As already mentioned, simulation was done only for the lower symmetry half of the turbine. Accordingly, only the lower halves of boundary and field lines are rendered. The boundary is rendered in gray and the torpedoes inside the injectors were omitted for better visibility.

In Fig. 11 to Fig. 14, the field lines are colored with distance to boundary to support the distinction between boundary flow and inner flow. Fig. 11 can be used to get a quick impression of the flow: Field lines near the boundary are colored blue whereas the usually more important field lines reaching the inner flow get different colors. Fig. 12 shows different flow features:

- We see high field line density at the right entrance of the first injector. According to the analysis in Section 4.1, we identify the large separation vortex and the smaller vortex caused by vortex sheet roll-up, passing over the separation vortex.
- At the second injector, we see vorticity lines that smoothly detach from the boundary of the manifold ring and join into the right part of the injector. In front of the right part of the injector, we also identify a backflow region indicated by quite vertical vorticity lines reaching the symmetry plane (refer to Fig. 13 for verification using streamlines). Fig. 13 also shows that the field lines detach roughly in direction of velocity (towards the
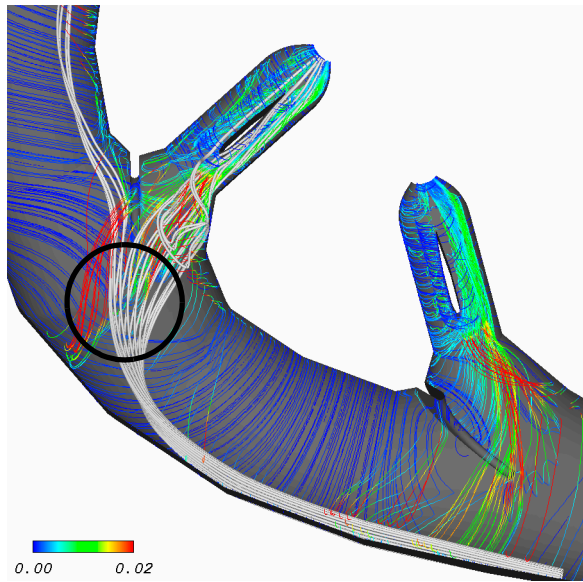
Figure 13: Closer look at the first two injectors, field lines again colored with distance to boundary. In the circled region, field lines detach roughly in direction of the streamlines (white tubes).
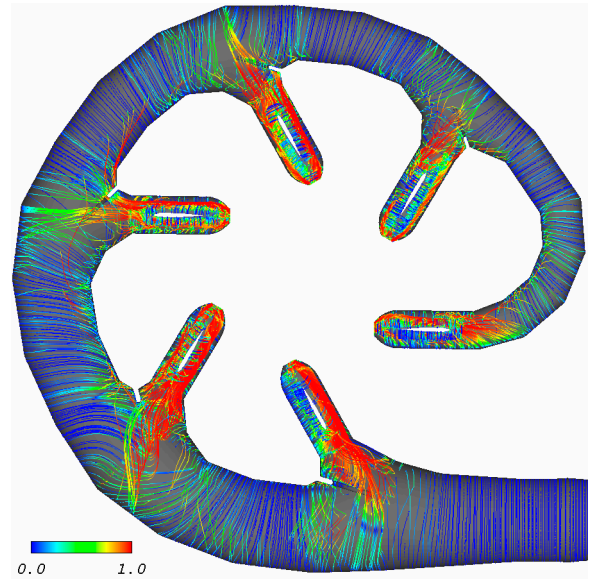

Figure 15: Top view of vorticity field lines colored with absolute value of normalized helicity.
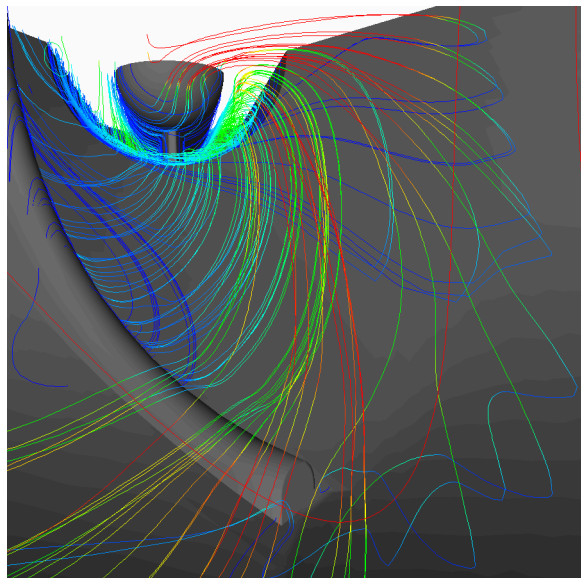

Figure 14: Close look at the first injector, field lines colored with distance to boundary. Some field lines follow the flow inside the injector while others connect to the boundary of the torpedo.

Figure 16: Closer look at the first two injectors, field lines colored with absolute value of normalized helicity.

injector). This indicates vorticity transport from the boundary layer.

Fig. 14 gives a close look at the first injector, lines are colored again by distance to boundary. We see that the field lines of the separation vortex follow the flow inside the injector, whereas the field lines of the vortex sheet roll-up connect to the boundary layer of the torpedo.
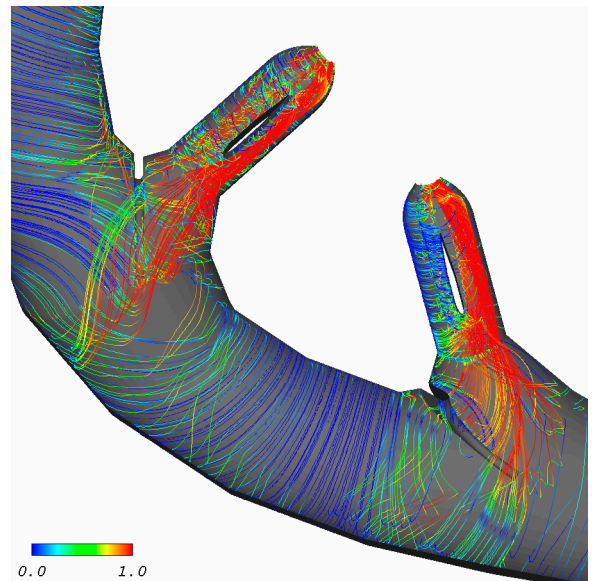
Fig. 15 and Fig. 16 show the same views, but this time the field lines are colored with normalized helicity to help the distinction between vortices (mainly red) and shear flow (mainly blue).

Fig. 17 and Fig. 18 show once more the same views, but this time the field lines are colored with vorticity magnitude. This type of visualization gives a more quantitative view of the vorticity field.

Table 1 contains some statistics of the line placement procedure. It has to be mentioned that, compared to the original algorithm of Turk and Banks, it took more time to adjust the parameters
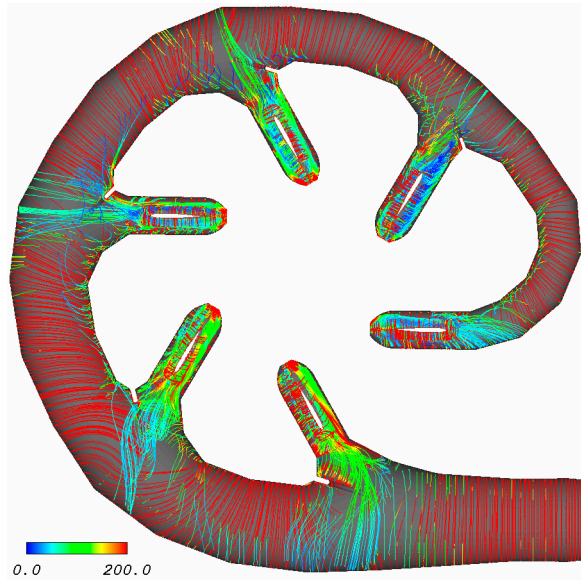
0.0   200.0

Figure 17: Top view of vorticity field lines colored with vorticity magnitude.
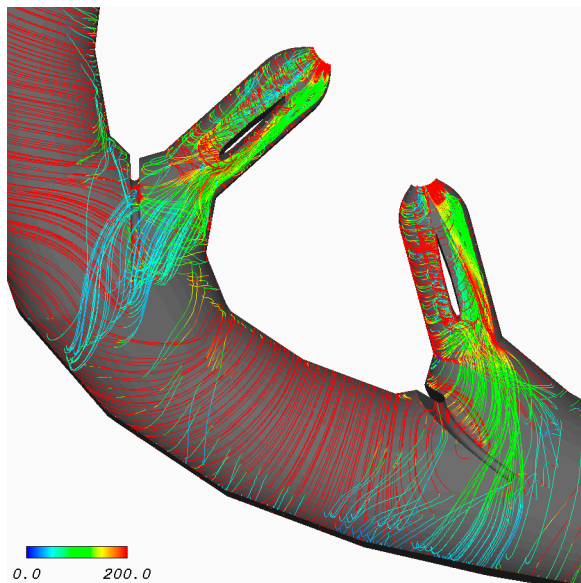

0.0   200.0

Figure 18: Closer look at the first two injectors, field lines colored with vorticity magnitude.

(scaling of the vorticity magnitude field, filter radius, random move radius) to obtain pleasant results. Because many node contributions of a given field line contribute to the same node of the low-pass field (due to several field line integration steps per grid cell and due to filter kernel size), multiple contributions to the same low-pass node are combined. For our dataset and algorithm settings, this resulted in a reduction of memory usage by one order of magnitude. The table shows counts of the already combined contributions.

Table 1: Statistics for the field line placement. Memory usage of the low-pass field is N_n and memory used by the field lines is $3N_v + N_c$.

Run	1	2	3
N_n = number of grid nodes		789132	
vorticity magnitude scale	0.003	0.005	0.005
iterations	10000	10000	40000
filter radius [m]	0.02	0.02	0.02
random move radius [m]	0.005	0.005	0.005
N_l = number of lines	1139	1541	2709
N_v / N_l = vertices per line	217.472	220.099	194.882
N_c / N_l = contributions per line	6404.75	6179.37	5668.7
initial energy	4.45526e+08	1.23757e+09	1.23757e+09
final energy	4.0472e+08	1.15074e+09	1.0707e+09
computation time [sec]	2460.43	2274.35	9673.02

5 CONCLUSION

We presented a field line placement algorithm for generating sets of field lines where the line density is proportional to the field magnitude. We found that the proposed visualization method is a useful tool for the investigation of vortical flow. In our belief, it visualizes vorticity and vortices in an appropriate manner, revealing interrelations and additional details. For speeding up the convergence of the line placement, we plan to implement an oracle to predict the most promising insertion or movement operations.

We also developed two visualization tools for the explorative analysis of velocity or vorticity fields. Based on extracted vortex core lines, the user can generate initially orthogonal circular stream tubes, by just a radius selection and a picking operation. Similarly, stream tubes can be generated from closed regions defined by one or two isosurfaces.

We believe that stream surfaces have been underestimated in their potential to explain complicated flow. Compared to sets of streamlines, stream tubes give better spatial perception. Beyond that, stream surfaces can even be inherent flow features, as in the case of separation surfaces. Beside Hultquist's original paper and a tetrahedra-based algorithm [26] we are aware only of one recent method [10], which we plan to implement as well. In our experience, stream surfaces as tools to assist vision are needed most in places where they are the most difficult to compute.

REFERENCES

[1] D. Banks, and B. Singer. Vortex Tubes in Turbulent Flows: Identification, representation, reconstruction. In *Proceedings of IEEE Visualization '94*, Computer Society Press, pp.132-139, 1994.

[2] G.K. Batchelor. An Introduction to Fluid Dynamics. *Cambridge University Press*, 1967.

[3] D. Bauer, and R. Peikert. Vortex Tracking in Scale-Space. *Joint Eurographics - IEEE TCVG Symposium on Visualization*, pp. 233-240, 2002.

[4] M.S. Chong, A.E. Perry, and B.J. Cantwell. A General Classification of Three-Dimensional Flow Fields. *Phys. Fluids*, A, 2(5):765-777, 1990.

[5] G.H. Cottet and P.D. Koumoutsakos. Vortex Methods: Theory and Practice. *Cambridge University Press*, 2000.

[6] W. De Leeuw and R. Van Liere. Collapsing Flow Topology Using Area Metrics. *Proceedings of IEEE Visualization '99*, IEEE Computer Society Press, pp. 349-354, 1999.

[7] Y. Dubief and F. Delcayre. On coherent-vortex identification in turbulence. *Journal of Turbulence*, http://jot.iop.org, vol.1, Dec. 2000.

[8] J. Ebling and G. Scheuermann. Clifford Convolution And Pattern Matching On Vector Fields. *Proceedings of IEEE Visualization 2003*, IEEE Computer Society Press, pp. 193 - 200, 2003.

[9] A. Fuhrmann, E. Gröller. Real-Time Techniques for 3D Flow Visualization. *Proceedings of IEEE Visualization 1998*, IEEE Computer Society Press, pp. 305-312, 1998.

[10] C. Garth, X. Tricoche, T. Salzbrunn, T. Bobach and G. Scheuermann. Surface Techniques for Vortex Visualization. To appear in *Data Visualization 2004*, Proc. of the Joint Eurographics - IEEE TCVG Symposium on Visualization, 2004.

[11] R. Haimes and D. Kenwright. On the Velocity Gradient Tensor and Fluid Feature Extraction. In *AIAA 14th Computational Fluid Dynamics Conference*, Paper 99-3288, 1999.

[12] J.L. Helman and Hesselink. Representation and Display of Vector Field Topology in Fluid Flow Data Sets. *IEEE Computer*, pp. 27-36, Aug. 1989.

[13] J.P.M. Hultquist. Constructing Stream Surfaces in Steady 3D Vector Fields. *Proceedings of IEEE Visualization '92*, pp. 171 – 178, 1992.

[14] J.C.R. Hunt, A.A. Wray and P. Moin. Eddies, Streams, and Convergence Zones in Turbulent Flows. *CTR Proc. of Summer Program 1988*, pp. 193-208, 1988.

[15] J. Jeong and F. Hussain. On the identification of a vortex. In *Journal of Fluid Mech.*, vol. 285, pp. 69-94, 1995.

[16] M. Jiang, R. Machiraju and D. Thompson. Geometric verification of swirling features in flow fields. *Proceedings of IEEE Visualization '02*, IEEE Computer Society Press, pp. 3307-314, 2002.

[17] B. Jobard and W. Lefer. Creating Evenly-Spaced Streamlines of Arbitrary Density. *Visualization in Scientific Computing '97*, Springer, pp. 43-56, 1997.

[18] Y. Levy, D. Degani and A. Seginer. Graphical Visualization of Vortical Flows by Means of Helicity. *AIAA* 28(8), pp. 1347-1352, 1990.

[19] H. Lugt. Vortex Flow in Nature and Technology. *Wiley*, 1972.

[20] X. Mao, Y. Hatanaka, H. Higashida and A. Imamiya. Image-Guided Streamline Placement on Curvilinear Grid Surfaces. *Proceedings of IEEE Visualization '98*, pp. 135 – 142, 1998.

[21] O. Mattausch, T. Theussl, H. Hauser and E. Gröller. Strategies for Interactive Exploration of 3D Flow Using Evenly-Spaced Illuminated Streamlines. *Proceedings of the 18th spring conference on Computer Graphics*, ACM Press, pp. 213-222, 2003.

[22] H. Miura and S. Kida. Identification of Tubular Vortices in Turbulence. *Journal of the Physical Society of Japan*, vol. 66, nr. 5, pp. 1331-1334, 1997.

[23] E. Parkinson, H. Garcin, C. Bissel, F. Muggli, A. Braune. Description of Pelton Flow Patterns with Computational Flow Simulations. *Hydro 2002,* Kiris, Turkey, Nov. 4-7, 2002.

[24] R. Peikert and M. Roth. The "parallel vectors" operator: a vector field visualization primitive. In *Proceedings of Visualization '99*, p.263-270, 1999.

[25] S.K. Robinson. Coherent Motions in the Turbulent Boundary Layer. *Ann. Rev. Fluid Mechanics*, 23:601-639, 1991.

[26] G. Scheuermann, T. Bobach, H. Hagen, K. Mahrous, B. Hamann, K.I. Joy and W. Kollmann. Tetrahedra-Based Stream Surface Algorithm. In *Proceedings of Visualization '01*, pp. 151-158, 2001.

[27] D. Silver and X. Wang. Volume Tracking. In *Proceedings of Visualization '96*, pp. 157-164, 1996.

[28] R.C. Strawn, D. Kenwright and J. Ahmad. Computer Visualization of Vortex Wake Systems. *American Helicopter Society 54th Annual Forum*, Washington DC, 1998.

[29] D. Sujudi and R. Haimes. Identification of Swirling Flow in 3D Vector Fields. *Tech. Report, Dept. of Aeronautics and Astronautics, MIT*, Cambridge, MA, 1995.

[30] X. Tricoche, G. Scheuermann, H. Hagen and S. Clauss. Vector and Tensor Field Topology Simplification on Irregular Grids. *Joint Eurographics - IEEE TCVG Symposium on Visualization*, pp. 107-116, 2001.

[31] G. Turk and D. Banks. Image-Guided Streamline Placement. *SIGGRAPH 1996*, pp. 453-460, 1996.

[32] V. Verma, D.T. Kao and A. Pang. A Flow-guided Streamline Seeding Strategy. In *Proceedings of IEEE Visualization '00*, IEEE Computer Society Press, 2000.

[33] VirCinity. http://www.vircinity.com, 2004.